

Investigation of the suitability of using modulated scatterers to measure the pattern of ground-penetrating radar antennas

Ricardo A. López¹ and Waymond R. Scott, Jr.
School of Electrical and Computer Engineering, Georgia Institute of Technology
Atlanta, GA, 30332-0250, USA

ABSTRACT

Experiments and simulations were performed in order to assess the suitability of electrically and optically modulated scatterers (OMS) as electromagnetic field probes for measuring the pattern of ground-penetrating radar (GPR) antennas. Of special importance for the probe are its comparative performance as well as its frequency response. The former is related to the depth of modulation that the modulating device is able to reach and can be optimized with a proper choice of active element. The latter was improved by making the probe more broadband. The present work will also show the steps that have been taken to achieve better frequency response from 2 GHz to 8 GHz by means of resistively loading the probe and discuss the trade-offs involved in doing so.

Keywords: modulated scatterer, optically modulated scatterer, ground-penetrating radar antenna, Wu-King profile

1. INTRODUCTION

The measurement of the radiation pattern in air is relatively straightforward. In contrast, measuring the underground pattern of ground-penetrating radar (GPR) antennas poses particular challenges. First, since GPRs are equipped with transmitting and receiving paths (separate antennas or a single antenna that serves both purposes), the combined pattern is the most useful. Clearly, a good probe must be able to backscatter part of the incident signal to make this pattern. This reveals the second challenge: the backscattered signal has to be somehow “flagged” at the probe so as not to be confused with other reflections that can occur as a result of inhomogeneities in the ground. One way to realize the above is with a *modulated scatterer* (MS), in which the probe is normally modulated at a frequency much less than the carrier frequency. The modulation is attained by means of an electronic component that loads the probe. This component can be modulated using electric current or light. The advantage of the optical approach is that the amount of spurious reflections that would occur from metallic cables is greatly reduced since a length of optical fiber can be used instead. The electrical approach has the advantage of being able to achieve deeper levels of modulation.

It should be kept in mind that GPR antennas for landmine detection must operate over wide bandwidths because they must have enough down-range resolution to accurately detect such devices. As such, the probes used to measure their pattern must be able to work on a similar range of frequencies. The traditional dipole probe is narrowband in nature but easy to build, making necessary the exploration of techniques to enlarge its bandwidth without adding complexity in its design. The outcome of one such method will also be shown here.

2. DEVICE SELECTION

The first task was to select a suitable photodiode to be used as the modulating element (ME). Some of the features to look for in the device are

- Small size,
- Symmetrical structure,

¹rlopezm@ieee.org

- Low impedance when turned on and high impedance when turned off,
- Operating wavelength compatible with that of commercially available infrared (IR) light sources,
- Easy and efficient attachment to an optical fiber.

After comparing PIN photodiodes from various manufacturers, the model FD80S7-F8 from Fermionics Inc. was chosen because of its small yet rugged layout and the fact that it is already pigtailed with a 62.5 μm /125 μm length of optical fiber. The source of IR light was built using the IR LED AMP TYCO 259012-1. The system operates at a wavelength of 1.3 μm . Pictures of the photodiode (with its leads extended) and the IR source are shown in Figure 1.

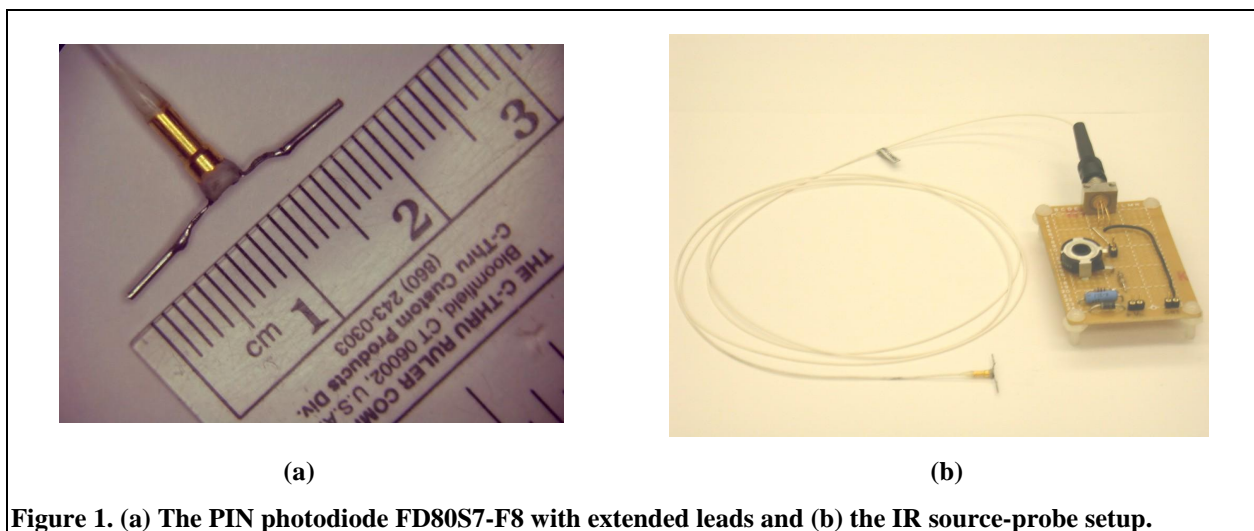


Figure 1. (a) The PIN photodiode FD80S7-F8 with extended leads and (b) the IR source-probe setup.

The photodiode impedance was experimentally measured using a vector network analyzer over the range from 2 GHz to 8 GHz and is presented in Figure 2. It was found that IR source currents above 60 mA did not provide a large change in the photodiode impedance and, therefore, this value was taken as the threshold to turn the diode on. It is clear that the photodiode's impedance varies strongly as a function of the incident light power, i.e., the modulating capability of the device was confirmed.

3. THEORETICAL CONSIDERATIONS AND FEASIBILITY TEST

An optically modulated scatterer (OMS) was built using the PIN photodiode with its dimensions shown in Figure 1.a. The symmetry of the device made it possible to build a dipole scatterer just by lengthening the photodiode leads up to 0.9 cm each. A 30 kHz square signal was used to modulate the photodiode. Cullen and Parr [1] proved that the voltage received by the homodyne detector is proportional to the square of the electric field at the probe location:

$$V_r = kE^2 .$$

The square of the electric field, in the case of an antenna, effectively represents the two-way pattern of the radiator and is of the utmost importance in this application. If the cross-section of the probe is a function of time (as a result of modulating it, for example), then the received voltage will show an additional component that varies in time:

$$\Delta V_r = \Delta kE^2 .$$

Therefore, we are interested in measuring the component of V_r that varies in time at the same rate as the modulated probe does, which for the present experiment is 30 kHz.

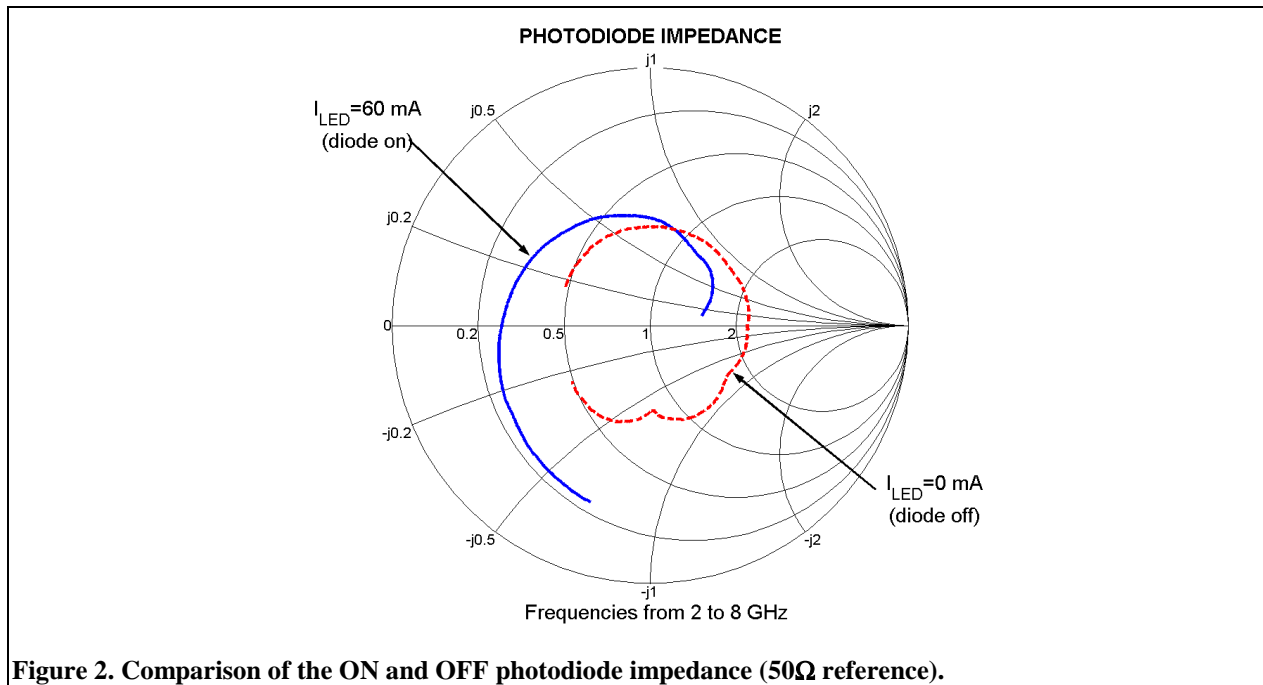


Figure 2. Comparison of the ON and OFF photodiode impedance (50Ω reference).

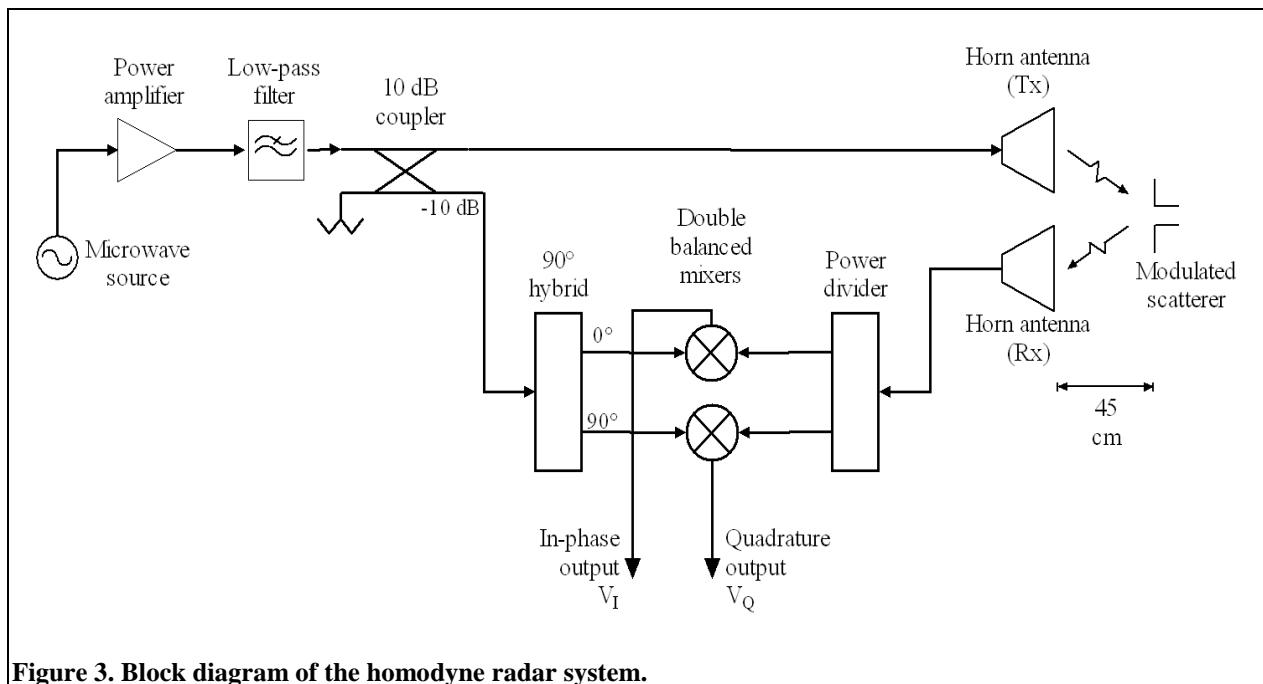


Figure 3. Block diagram of the homodyne radar system.

The received voltage contains modulated and unmodulated components and can be written as

$$V_r = [A + \Delta A(t)]\cos[\omega t + \varphi + \Delta\varphi(t)] + A_c\cos(\omega t + \varphi_c), \tag{1}$$

where A and φ account for unmodulated components in amplitude and phase, respectively, arising from the probe; $\Delta A(t)$ and $\Delta\varphi(t)$ are the small amplitude and phase modulation introduced by the modulated probe, respectively, at

30 kHz; while A_c and φ_c are the amplitude and phase of the undesired coupling between the antennas and includes reflections from the surroundings as well. If the probe were not modulated, its backscattering would be buried in this relatively large component, making the detection unreliable.

A schematic diagram of the bistatic (separate transmitting and receiving antennas) homodyne radar system used in this experiment is shown in Figure 3. This radar was previously built to measure displacements of the surface of the earth and mines due to elastic waves [10]. The microwave source used was a sweep oscillator from 2 GHz to 8 GHz and the amplitude of the low-frequency component output (corresponding to the probe-modulating signal frequency) was recorded. A photograph of the antenna-probe setup is shown in Figure 4.

At the output of the radar, the in-phase and quadrature components are

$$\begin{aligned} V_I &= A \cos(\varphi) + A_c \cos(\varphi_c) + v_I(t) \quad , \quad v_I(t) = M(t) \sin[\varphi + \theta(t)] \\ V_Q &= -A \sin(\varphi) - A_c \sin(\varphi_c) + v_Q(t) \quad , \quad v_Q(t) = M(t) \cos[\varphi - \theta(t)] \end{aligned} \quad (2)$$

where

$$M(t) = |\Delta\varphi(t)| \sqrt{A^2 + \left[\frac{\Delta A(t)}{\Delta\varphi(t)} \right]^2}$$

$$\theta(t) = -\arctan \left[\frac{1}{A} \frac{\Delta A(t)}{\Delta\varphi(t)} \right]$$

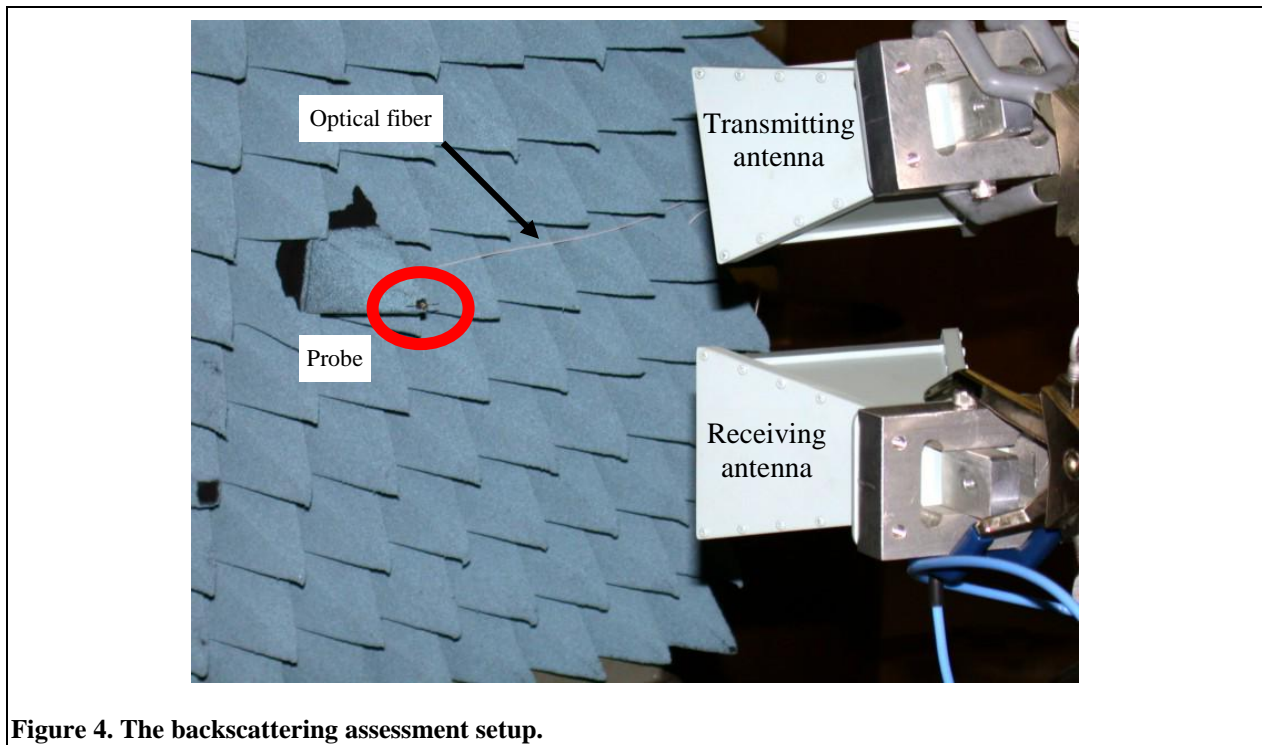


Figure 4. The backscattering assessment setup.

Since the angle $\theta(t)$ was observed to be small, the magnitude of the 30 kHz component can be found by using

$$R = \sqrt{|v_I(t)|^2 + |v_Q(t)|^2} \quad (3)$$

The spectrum around 30 kHz of one of the radar outputs is shown in Figure 5. The 30 kHz component, R, is seen to be well above the noise floor (by approximately 40 dB), enough so as there should be no problems in detecting and measuring it.

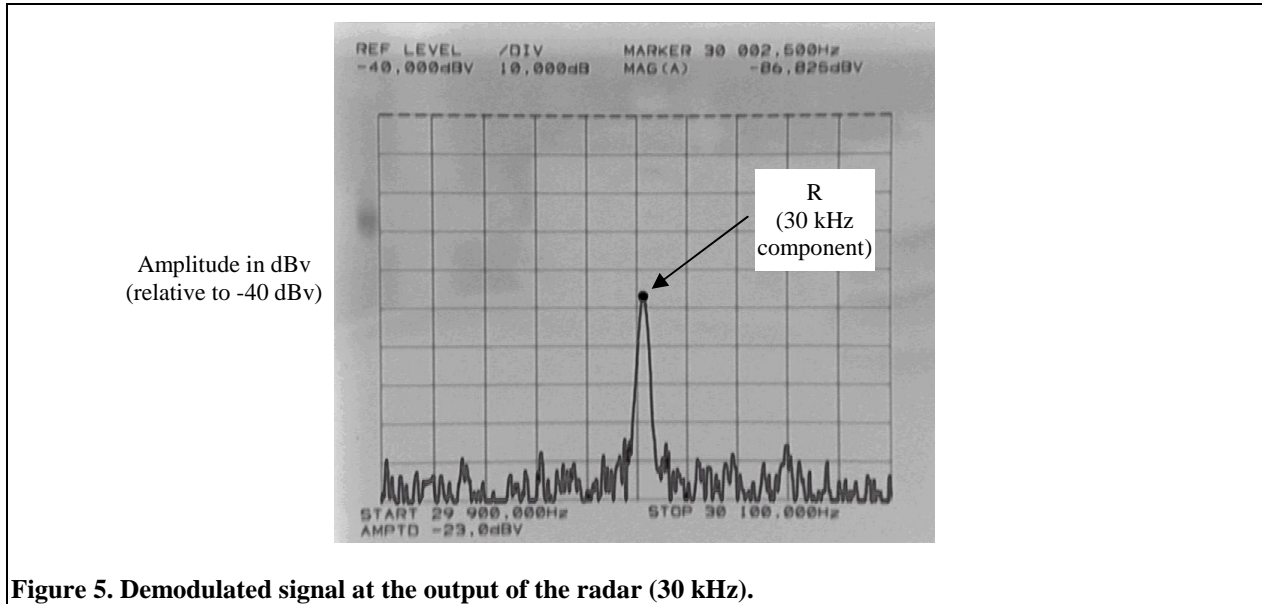


Figure 5. Demodulated signal at the output of the radar (30 kHz).

4. SIMULATIONS AND BANDWIDTH IMPROVEMENT

One drawback of using a dipole as a probe is its frequency response. Since the dipole is a resonant structure, its frequency response peaks at specified frequencies and therefore some technique to improve bandwidth is required. The main reason for this need of larger bandwidth is the present application related to GPR antennas. The GPR pulses are rich in frequency content (broad spectrum) and in order to be transmitted adequately, the GPR antennas have to keep the pulse shape as close to the original as possible, so these are generally broadband antennas. If a probe is meant to measure the pattern of this type of antennas, it also has to have a reasonably good frequency response. A possible solution is to shape the antenna so as to make it frequency independent [3]. However, this approach would require a larger probe, which will affect the field under test. A better solution is to resistively load the dipole, as proposed by Wu and King [4]. This method replaces the metallic arms of the probe by a conductive material whose resistivity per unit length (R_L) varies along the arms according to the profile shown in Equation 4, where the dipole is assumed to be centered at the origin and aligned along the z -axis, and where h represents the length of each of the arms. ψ is a parameter defined in [4].

$$R_L(z) = \frac{R_0}{1 - \left|\frac{z}{h}\right|}, \quad R_0 = \frac{\eta_0 \psi}{2\pi h} = 21766 \text{ } \Omega/m \quad (4)$$

For practical purposes, however, it is convenient to discretize Equation 4. This has been done in two ways: using a discrete surface impedance gradient and using lumped resistors along the metallic dipole.

4.1 Discrete surface impedance gradient

The dipole was discretized to simulate its backscattering properties using an electromagnetics simulator. Also, in preparation for future probe implementation on a printed circuit board substrate, the cylindrical dipole was converted to an equivalent flat one (tape-shaped). Figure 6 depicts the discretized geometry, composed of 30 segments, each being 1 mm long.

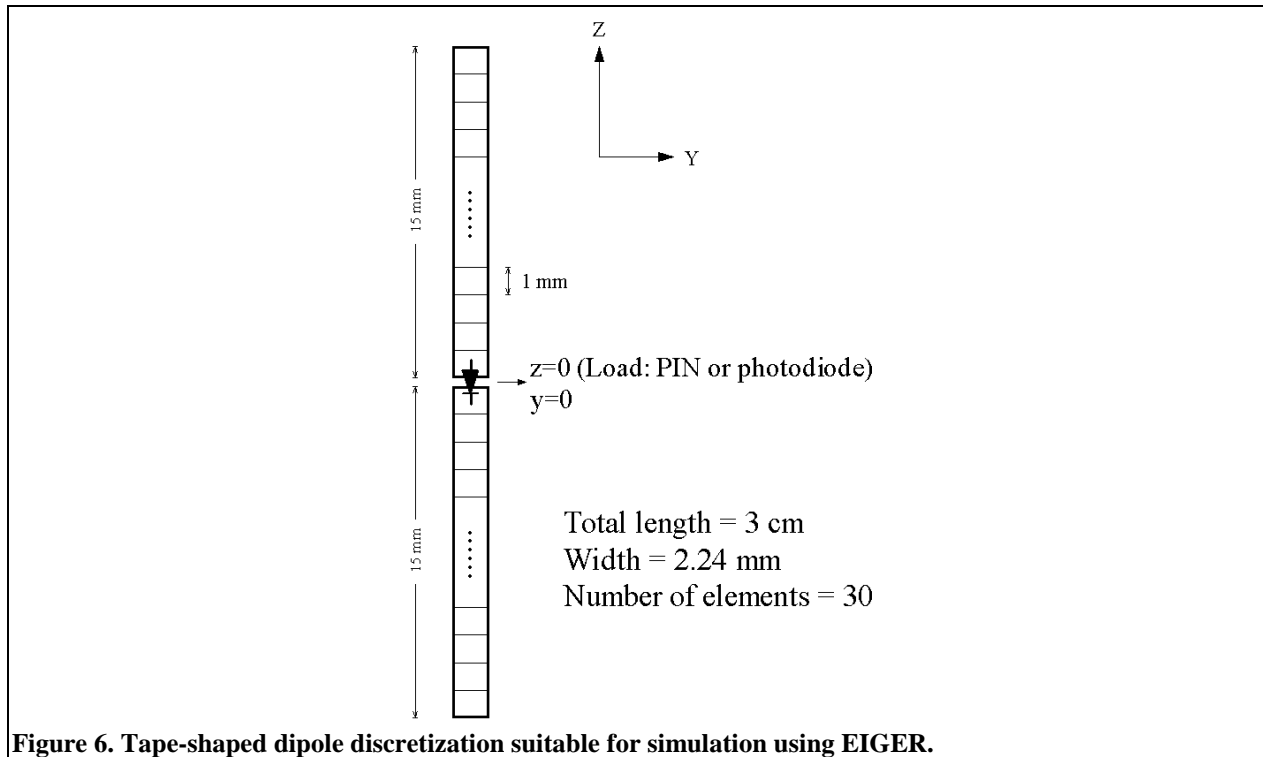


Figure 6. Tape-shaped dipole discretization suitable for simulation using EIGER.

The simulator requires a value of surface impedance (ρ_s , units of ohms per square) to be assigned to each element. Therefore, the discretized equation is

$$\rho_{s,i} = R_L(z = z_i) \cdot W(z = z_i) \quad (5)$$

where

- z_i : z-coordinate of the center of the i^{th} element
- $\rho_{s,i}$: discretized value of surface impedance for the i^{th} element
- $W(z = z_i)$: width of the i^{th} element
- $R_L(z = z_i)$: discrete value of resistance per unit length at z_i

Because of the symmetrical geometry, only the values for the upper arm have to be computed. The corresponding values for the lower arm are the same.

4.2 Lumped Elements

Using this approach, the elements were modeled as perfect conductors with resistors placed between them to approximate the continuous resistive loading. From the definition of resistance, and proceeding only for the upper arm of the dipole ($z > 0$),

$$r_i = 326,5 \ln \left| \frac{0,015}{0,015 - z_i} \right|. \quad (6)$$

Since the Wu-King profile is symmetrical, similar values of resistance were used for the corresponding elements in the lower arm ($z < 0$).

4.3 Simulation Results

Figure 7 shows the comparison between the amplitudes of the demodulated signals at the output of the radar (R in

equation 3), when *metallic* and *resistively loaded* dipoles were simulated. Even though the latter case shows a lower amplitude (less amount of backscattering), it also provides a significant improvement in the frequency response, which is flatter. Therefore, the resistive loading approach works in flattening the frequency response of the MS, at the cost of reduced backscattering efficiency.

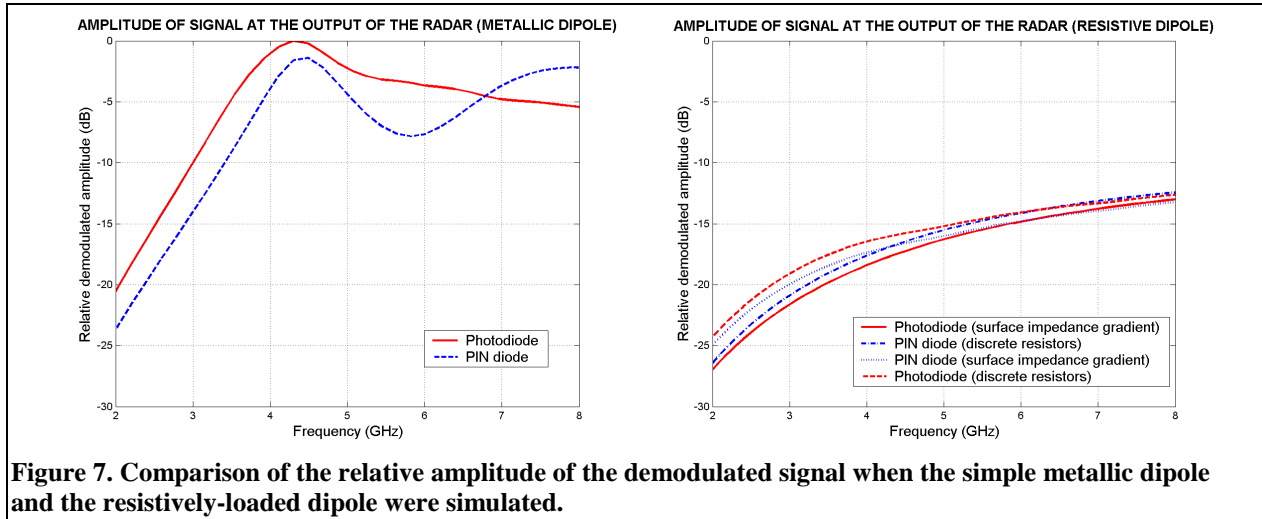


Figure 7. Comparison of the relative amplitude of the demodulated signal when the simple metallic dipole and the resistively-loaded dipole were simulated.

4.4 Continuously resistively-loaded dipoles

Additional simulations have been carried out considering the case of a dipole made of a resistive material instead of copper and discrete resistors. In this case, the Wu-King profile is achieved by shaping the arms of the dipole linearly (triangular shape), according to the following derivation:

$$W(z) = \frac{\sigma_s}{2R_0} \left(1 - \frac{z}{h} \right) \quad (7)$$

where σ_s : resistivity of the material in Ω/\square
 $W(z)$: width of the dipole at z , $-h \leq z \leq h$

The base of the triangle corresponds to the center of the dipole. The results of these simulations in EIGER are shown in Figure 8 (obtained for $\sigma_s = 25 \Omega/\square$). The performance of these probes is very close to the ones using the discretized version in sections 4.1 and 4.2, suggesting that the discretized models approaches very accurately the ideal continuous case of the Wu-King profile.

Also shown in Figure 8 is a simulation where the resistive material was replaced by a triangular patch of copper (referred to as metallic in the legend) and having a PIN diode as the modulating element. A photograph of this probe can be seen in figure 12. Interestingly, the response of the metallic probe does not exhibit peaking at the lower frequency range. This results will be verified by building the probes and testing them (refer to section 5.4).

4. IMPLEMENTATION

The following types of probes have been built on printed circuit boards (FR-4 material with 0.5 ounce copper foil):

5.1 Simple dipole

Two dipoles, 3 cm long, were made, one being loaded by the photodiode and the other by the PIN diode HPND 4005. Photographs of these probes can be seen in Figures 9 and 11, respectively. These will also serve as references for the performance of the rest of probes.

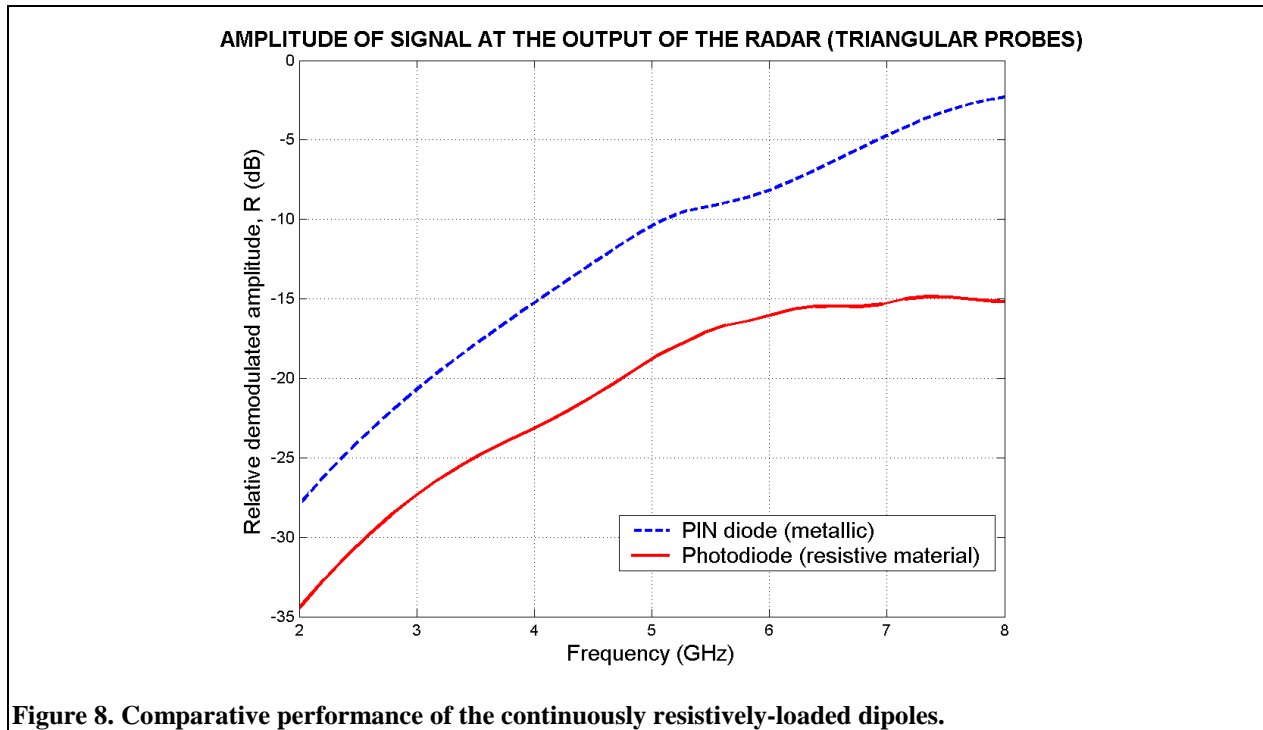


Figure 8. Comparative performance of the continuously resistively-loaded dipoles.

The electrical version (EMS) requires the addition of feeding lines to bias the PIN diode. The diode will be fed from a signal generator with a 30 kHz square signal via a pair of twisted wires. It is important to prevent RF leakage from the dipole into the signal generator and the wires. This has been achieved using a symmetrical first order low-pass RC network with a cutoff frequency of 1.5 MHz. Refer to Figure 11 for the layout of the feeding lines.

5.2 Optical discrete surface impedance gradient probe

This is a direct implementation of Figure 6, with the SMD resistors placed in between the elements that make the dipole up. A photograph can be seen in Figure 10. Eighteen resistive elements were used.

5.3 Electrical discrete surface impedance gradient probe

Similar to the previous, but this time using the HPND 4005 as the load. In this case, feeding lines as described in 4.4 are also included. Figure 11 depicts this probe.

5.4 Triangular probe

In order to verify the results of section 4.4, optical and electrical versions of the metallic triangular probes, 3 cm long, were built. One of them (optical probe) is shown in figure 12.

The setup used to evaluate the performance of these probes is similar to the one shown in Figures 3 and 4. The in-phase and quadrature outputs of the radar were measured and the amplitude of the modulated component, R, was computed and is shown in Figure 13. Figure 13.a corresponds to the different types of EMSs (3cm rectangular, 3cm triangular and discrete Wu-King profile), while Figure 13.b corresponds to the OMSs (3cm rectangular, 3cm triangular and Wu-King profile).

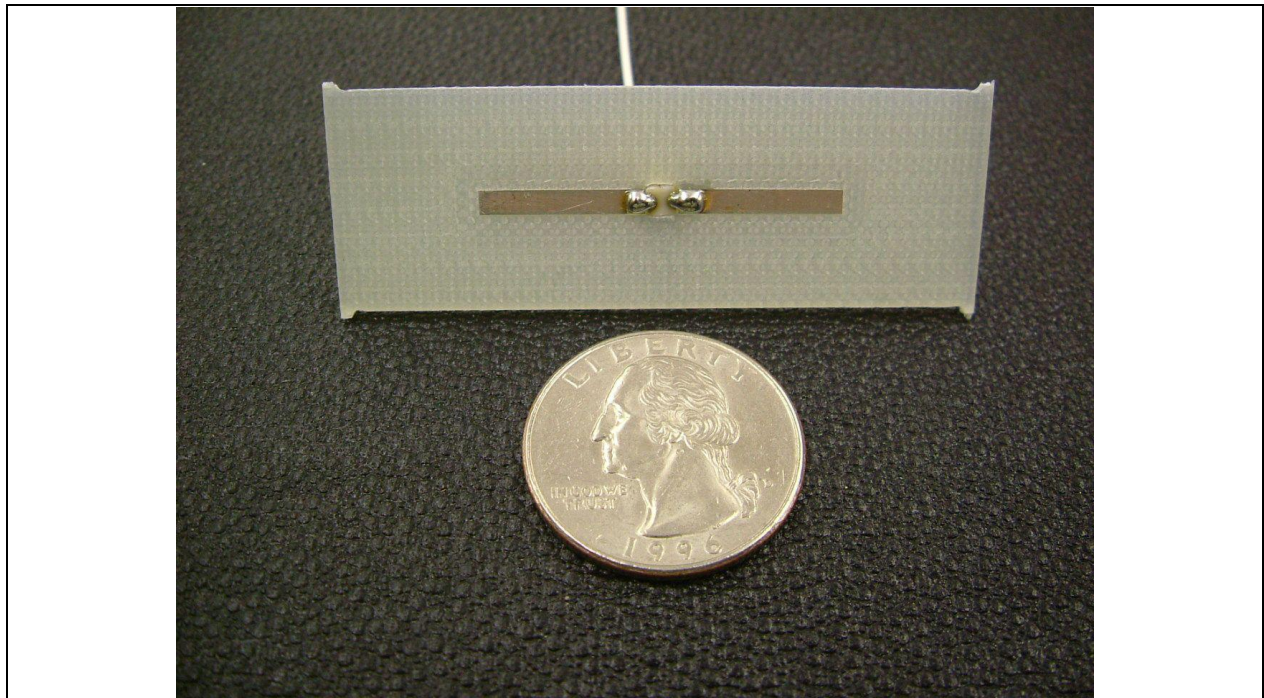


Figure 9. Simple optical probe, 3 cm long. Note the optical fiber leaving the probe from underneath it.



Figure 10. Resistively-loaded optical probe, 4 cm long.

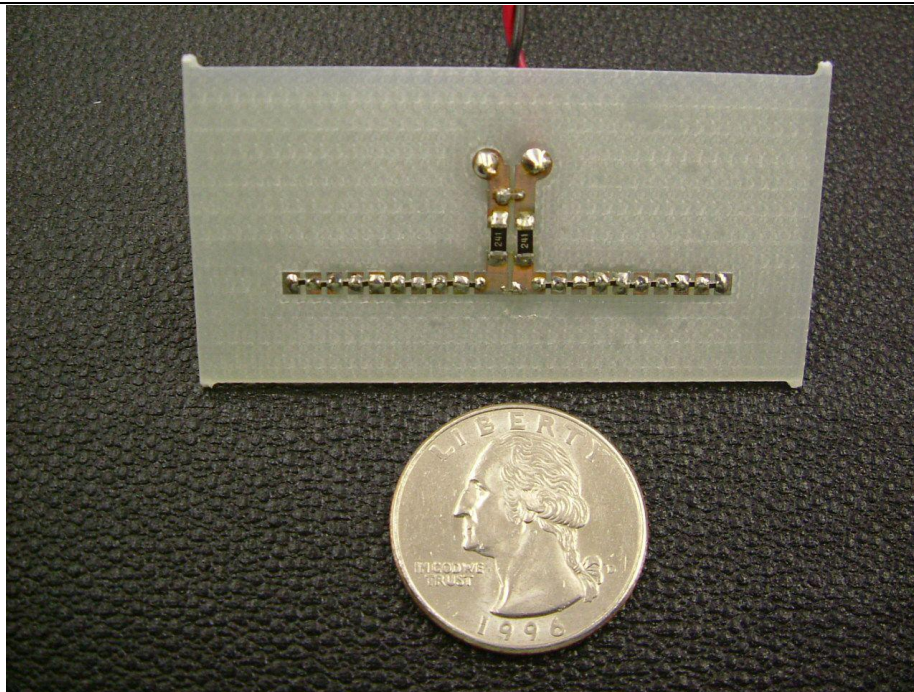


Figure 11. Resistively-loaded electrical probe, 3 cm long, showing the low-pass feeding lines.

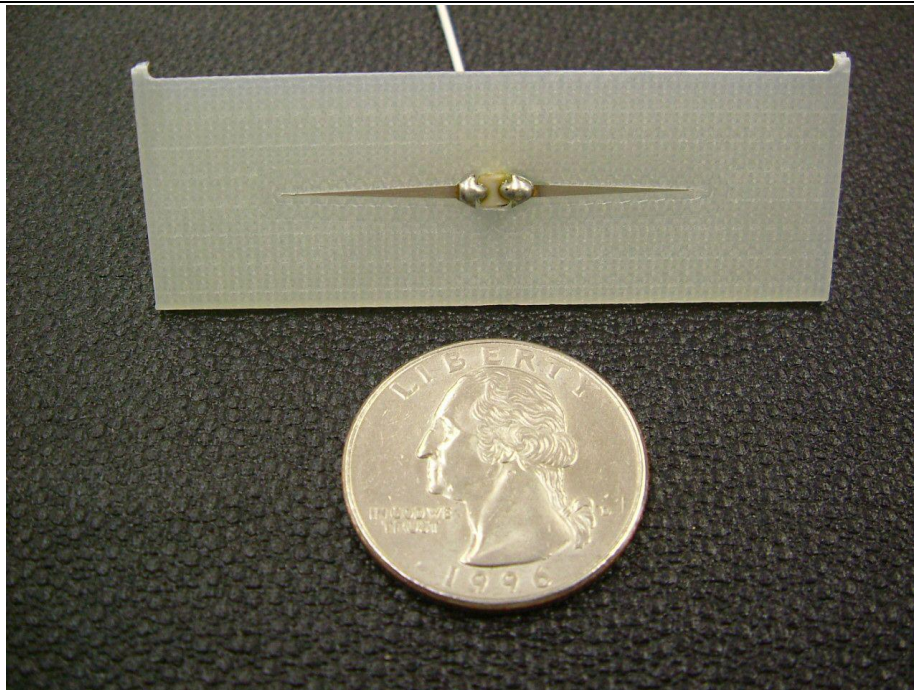


Figure 12. Metallic triangular optical probe, 3 cm long.

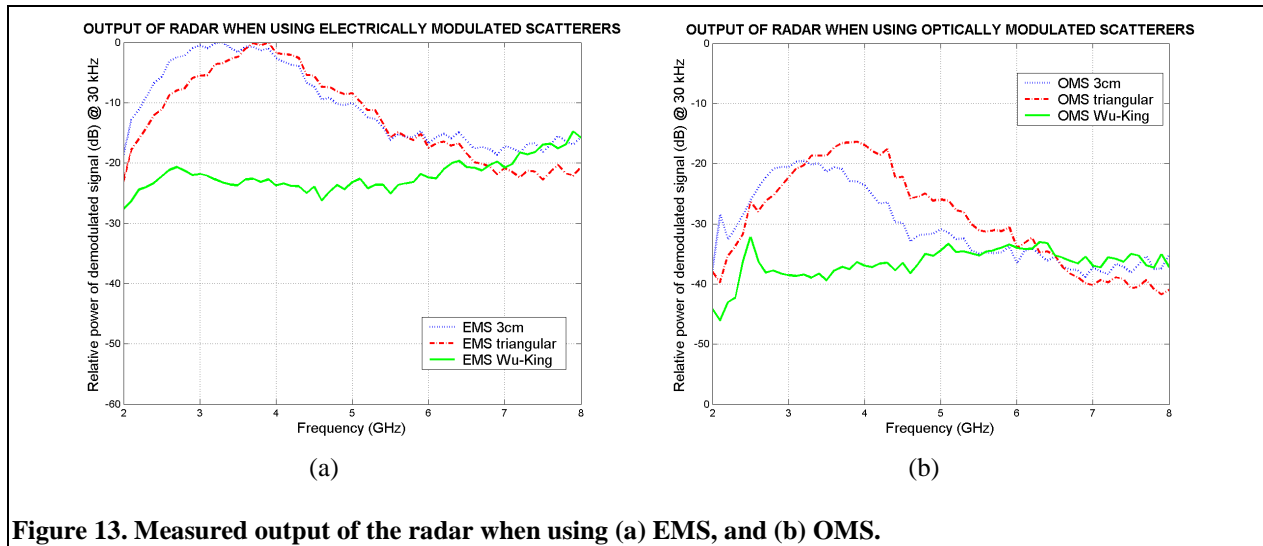


Figure 13. Measured output of the radar when using (a) EMS, and (b) OMS.

The measured difference in backscattering efficiency between the EMS and OMS is in good agreement with the simulation results. However, there is a discrepancy in the frequency response, particularly in the cases when no resistive loading was used (3cm metallic and triangular metallic probes). This is believed to be caused in part by differences in the models for the PIN and photodiode used in the simulations which becomes less accurate due to increased parasitic components as frequency increases. Interestingly, the peaks in response for both, OMS and EMS, happen at approximately the same frequencies, which suggest that the geometry of the probes has a heavier bearing at this respect. The resistively loaded probes, on the other hand, do show a more uniform frequency response. The loss of efficiency, though, is seen to be the worse between 2 and 5 GHz, and becomes smaller as the frequency increases, basically because the other probes' response worsen at higher frequencies. While such a roll-off at higher frequencies is expected from simulations, the actual one is larger and deserves more investigation.

5. CONCLUSIONS AND FUTURE WORK

Experiments have proven the suitability of the MSs as field probes. They help to improve the SNR when a low frequency modulating signal is used (30 kHz was used here). The problem of nonuniform frequency response was partially solved by resistively loading the probe according to the Wu-King theory, at the expense of backscattering efficiency. Future work will focus on testing other profiles besides the one proposed by Wu and King in order to increase the radar cross-section without sacrificing much bandwidth. Also, underground measurements will be taken to assess the usefulness of the electrical and optical MSs in the accurate measurement of the combined (bidirectional) pattern of GPR antennas.

ACKNOWLEDGEMENTS

This work is supported by the US Army Night Vision and Electronic Sensors Directorate, Science and Technology Division, Countermine Branch.

REFERENCES

1. A. M. Cullen and J. C. Parr, "A new perturbation method for measuring microwave fields in free space," *Proc. IEE*, vol. 102b, pp. 836-844, 1955.
2. J. C. Bolomey and F. E. Gardiol, *Engineering Applications of the Modulated Scatterer Technique*. Norwood, MA: Artech House, 2001.
3. C. A. Balanis, *Antenna Engineering*. New York, NY: John Wiley & Sons, 1997.
4. T. T. Wu and R. W. P. King, "The cylindrical antenna with nonreflecting resistive loading," *IEEE Transactions on Antennas and Propagation*, vol. AP-13, pp. 369-373, May 1965.
5. D. Slater, *Near-Field Antenna Measurements*. Norwood, MA: Artech House, 1991.
6. G. Hygate and J. F. Nye, "Measuring microwave fields directly with an optically modulated scatterer," *Measurement Science and Technology*, vol. 1, pp. 703-709, 1990.
7. Fermionics, Inc., "Type S7 Package (High Speed Mini-Pigtail) [p/n FD80S7-F]." [Online document], 2003, Available HTTP: <http://www.fermionics.com/S7pic.htm>.
8. Seung-Ho Lee, *Measurement of Time-Varying Surface Displacements using a Radar*. Doctoral Thesis in Electrical and Computer Engineering, Georgia Institute of Technology, Atlanta, GA, 2002.
9. D. M. Pozar, *Microwave Engineering*. New York, NY: John Wiley & Sons, 1998.
10. W. R. Scott, Jr., C. T. Schröder and J. S. Martin, "An acousto-electromagnetic sensor for locating land mines", *Detection and Remediation Technologies for Mines and Minelike Targets III, Proc. SPIE*, April 1998, vol. 3392, pp. 176-186.